Convective and Tectonic Plate Velocities in a Mixed Heating Mantle

A. Lenardic, J. Seales, W. Moore, M. Weller

Department of Earth Science, Rice University, Houston, TX 77251-1892. (ajns@rice.edu)

Abstract

Mantle convection and, by association, plate tectonics is driven by the transport of heat from a planetary interior. This heat comes from the internal energy of the mantle and from heat flowing into the base of the mantle from the core. Past investigations of such mixed-mode heating have revealed unusual behavior that confounds our intuition based on end-member cases. In particular, increased internal heating leads to a decrease in convective velocity. We investigate this behavior using a suite of numerical experiments and develop a scaling for velocity in the mixed-heating case. We identify a planform transition, as internal heating increases, from sheet-like to plume-like downwellings that impacts heat flux and convective velocities. More significantly, we demonstrate that increased internal heating leads not only to a decrease in internal velocities but also a decrease in the velocity of the upper thermal boundary layer (a model analog of the Earth's lithosphere). This behavior is connected to boundary layer interactions and is independent of any particular rheological assumptions. In cases with a temperature-dependent viscosity and weak plate margin analogs, increased internal heating does not cause an absolute decrease in surface velocity but does cause a decrease relative to purely bottom or internally heated cases as well as a transition to rigid-lid behavior at high heating rates. The differences between a mixed system and end-member cases have implications for understanding the connection between plate tectonics and mantle convection and for planetary thermal history modeling.

Keywords: Plate Tectonic Velocity, Mantle Convection, Mixed Heating, Planetary Cooling

1. Introduction

Thermal convection in the Earth's mantle is driven in two ways: 1) Internal heating from the decay of radioactive elements in the mantle or bulk cooling and 2) Heat flowing into the base of the mantle from the Earths' core (basal heating) [Schubert 2001]. Numerous studies have explored the dynamics of convection driven by mixed heating [Schubert and Anderson, 1985; Grasset and Parmentier, 1998; Sotin and Labrosse, 1999; Moore, 2008; Shahnas et al., 2008; Choblet and Parmentier, 2009; Wolstencroftet al., 2009; O'Farrell and Lowman, 2010; Choblet, 2012; Deschamps et al., 2010; 2012; O'Farrell et al., 2013; Stein et al., 2013; Weller et al., 2015; Korenaga, 2017]. The studies have elucidated similarities and differences between mixed mode heating and end-member cases of internal or basal heating. This study is motivated by a difference noted by O'Farrell and Lowman [2010].

Figure 1a is reproduced from O'Farrell and Lowman [2010]. Their numerical experiments, in a 3D Cartesian domain, showed that as the degree of internal heating increased, for a mixed heating system, the root mean square (rms) velocity of the system decreased. This is surprising as an increase in internal heating is associated with an increase in the internal heating Rayleigh number. Given that a Rayleigh number expresses the ratio of forces driving to forces resisting convection, one might expect the opposite behavior, i.e., enhanced convective vigor and increased system velocity. It was subsequently shown that the trend of decreasing velocity with increasing internal heating holds in spherical geometry as well [Weller et al., 2016; Weller and Lenardic, 2016]. Figure 1b documents this geometric robustness.

O'Farrell and Lowman [2010] argued that decreasing rms velocity was due to thermal upwellings becoming more diffuse with increased internal heating [Jellinek et al., 2002]. In the bottom heating end-member, upwellings are concentrated plumes originating from a lower thermal boundary layer. In the internally heated end-member no lower boundary layer exists and upflows are broad regions of return flow. Increased internal heating increases internal mantle temperature which, for fixed basal temperature, lowers the heat flux into the mantle. In effect, the contribution of bottom heating decreases [Moore, 2008], even though the bottom-heated Rayleigh number is unchanged. This causes a transition from high velocity, concentrated thermal upwellings (plumes) to broad, low velocity upwelling zones (passive return flow). This effect should also hold if the surface boundary layer becomes more diffuse and O'Farrell and Lowman [2010] ran cases with internal cooling

(negative internal heating) to show that this is the case (Figure 1a).

The explanation above relies solely on the lower boundary layer and its response to increased internal heating. However, the behavior of the upper boundary layer is also affected by the change in internal temperature and the decrease in plume buoyancy flux arriving from the other layer [Moore, 2008]. While O'Farrell and Lowman [2010] identify changes in rms velocity, the effects on surface velocity are more relevant for understanding plate tectonics and planetary cooling. This leads to the question of wether the trend mapped by O'Farrell and Lowman [2010] also holds for surface velocity. This sets the motivation for what follows herein. We will begin by presenting a theoretical argument, based on Moore [2008], as to why decreasing surface velocities are to be expected. From there we will move to suites of numerical experiments.

Our experiments will begin, following O'Farrell and Lowman [2010], by considering iso-viscous convection in a three-dimensional, Cartesian domain. We then perform a suite of two-dimensional simulations which allow us to explore the effects of changing cell aspect ratios (this can show the degree to which velocity trends depend on changes in convective planforms). Finally, we consider cases that allow for temperature-dependent viscosity and the formation of weak zones that serve as analogs for plate boundaries. We conclude with a discussion of the implications of mixed-mode convection for planetary thermal evolution.

2. Theoretical Expectations

Mixed heated convection is governed by a bottom heating Rayleigh number:

$$Ra = \frac{\rho g \alpha \Delta T D^3}{\kappa \eta}, \tag{1}$$

and a heating ratio:

$$Q = \frac{Ra_i}{Ra} = \frac{\rho H D^2}{\Delta T k}, \tag{2}$$

where ρ is the mantle density, g is the gravitational acceleration, α is the coefficient of thermal expansion,ΔT is the temperature drop across the system, D is the system depth, κ is thermal diffusivity, η is viscosity, Ra_i is the Rayleigh number defined for internal heating, H is internal heat generation per unit mass, and k is thermal conductivity.

Classical convective scalings assume that thermal boundary layers behave in a self-determined manner [Howard, 1966]. The scalings are derived by

assuming that a local stability criteria governs the thickness of boundary layers. A local Rayleigh number, Ra_δ, can be defined for the upper thermal boundary layer as

$$Ra_\delta = \frac{\rho g \alpha \left(T_i - T_s\right) \delta^3}{\kappa \eta} \tag{3}$$

where δ is the boundary layer thickness. If the surface temperature T_s is constant, then T_i, the internal temperature of the convecting layer, provides a measure for the temperature drop across the boundary layer. When Ra_δ exceeds a critical value, Ra_c, convective instabilities form and the lower portions of the boundary layer detach. This acts to maintain the boundary layer at a critical thickness and a statistically steady state is achieved with $Ra_\delta = Ra_c$. As a result, the critical boundary layer assumption predicts that $\delta \sim Ra^{-1/3}$. A second prediction is that increased internal temperature, which increases Ra, decreases δ according to $\delta \propto \Delta T^{-1/3}$.

We can connect δ to boundary layer velocity (u) by considering the balance between conductive and advective time scales. The time it takes heat to diffuse across the boundary layer is given by τ. We then have $\delta = \sqrt{\kappa \tau}$. An advective time scale can be defined as aD/u, where a is the aspect ratio of a convection cell. If the boundary layer becomes unstable at a critical thickness, which limits the cell aspect ratio, then the two time scales are equal and $\delta \propto u^{-1/2}$. This amounts to applying Howards criteria [1966] to cellular convection. Boundary layer theory, which explicitly solves for boundary layer velocity as a function of aspect ratio, leads to an equivalent scaling relationship between δ and u [Turcotte and Oxburgh, 1967]. Relating this to our earlier expression, we see that $u \propto \Delta T^{2/3}$. Increasing internal temperature is thus predicted to increase boundary layer velocity. The thermal history community has leaned on this prediction for decades [Davies, 1980; Schubert et al., 1980]. It is a reason why a decrease in upper boundary layer velocity, with increased internal heating in an iso-viscous layer, has not been looked for to date in the context of numerical and/or laboratory experiments.

If boundary layer velocity can decrease with increased internal heating then the concept of self-determined boundary layer behavior may be incomplete. For bottom heated, high Reynolds number convection it has been shown that a self-determined boundary layer regime is not achieved even at what are considered to be very high Rayleigh numbers [Castaing et al., 1989]. This behavior has been attributed to an "inertial wind" that shears the upper boundary layer and prevents it from achieving a critical thickness

[Kadanoff, 2001]. Although inertial effects are absent in mantle convection, boundary layer interactions can occur [Weinstein et al., 1989; Lenardic and Kaula, 1994; Labrosse, 2003]. Moore [2008] has argued that such interactions could also short-circuit self-determined boundary layer behavior. Although, Moore [2008] did not explicitly present a prediction for boundary layer velocity, it is implicit within his theory that boundary layer velocity can decrease with increased internal heating (as shown below).

The concept of a self-determined boundary layer assumes that there is no interaction between upper and lower boundary layers. At very high degrees of convective vigor this will be achieved as, for example, upwelling plumes will dissipate before they impact the upper boundary layer. Moore [2008] noted that, under general conditions, there is no predicted value of Ra required for this. He further noted that discrepancies between classic scaling predictions and experimental results, even at values considered to be "high" Ra, indicated that mantle convection may not reach the self-determined boundary layer limit. For example, the numerical experiments of Lenardic and Moresi [2008] indicated that classic scaling trends were only approached asymptotically for $Ra > 10^9$. If boundary layers do interact then this could prevent the upper thermal boundary layer from reaching a critical thickness as per the theory of Howard [1966]. All other factors being equal, a decrease in boundary layer interaction could lead to upper boundary thickening and, by association, a decrease in boundary layer velocity. Increased internal heating, in a mixed heated layer, could progressively reduce boundary layer interactions as thermal upwelling become weaker and can no longer impede the upper thermal boundary layer from growing to a critical thickness [Labrosse, 2003].

The conceptual idea above can be formalized using the theory of Moore [2008]. The theory, and associated numerical experiments, predict that the temperature drop across the upper thermal boundary layer (ΔT_{top}) scales as

$$\Delta T_{top} = 0.499 + 1.33 Q^{3/4} Ra^{-1/4} \tag{4}$$

and that the non-dimensional heat flow (Nu) across the upper boundary scales as

$$Nu_{top} - 1 = Nu_{bot} - 1 + Q = 0.5Q + 0.206(Ra - Ra_c)^{0.318}. \tag{5}$$

An upper boundary layer thickness (δ) can be derived from the ratio of these two. Recalling that $\delta \sim u^{-1/2}$, we predict that the upper boundary velocity

scales as

$$\frac{u}{U} = \left(\frac{0.5Q + 0.206(Ra - Ra_c)^{0.318}}{0.499 + 1.33Q^{3/4}Ra^{-1/4}} \right)^2 \tag{6}$$

where U is a scaling constant. The scaling theory predicts that regions exist, within Ra and Q parameter space, over which increased internal heating leads to a decrease in upper boundary layer velocity. This occurs despite the fact that surface heat flux increases. That type of behavior is distinctly different from classic ideas about the connection between mantle heat loss and upper boundary layer velocity [Turcotte and Oxburgh, 1967]. The velocity scaling above is not explicitly found in Moore [2008] and upper boundary layer velocities were not tracked. We will do so in the numerical experiments that follow to test the ideas above.

3. Numerical Experiments: Methods

Our numerical experiments are defined by equations of mass, momentum, and energy conservation/balance for mixed heating mantle convection under the Boussinesq approximation. The non-dimensional equations are given by:

$$\partial_i u_i = 0 \tag{7}$$

$$\partial_j [2\eta(T, \tau_{yield}, I)\epsilon_{ij}] = \partial_i p + RaT\hat{k} \tag{8}$$

$$\partial_t T + u_i \partial_i T = \partial_i{}^2 T + H \tag{9}$$

$$\rho = [1 - \alpha(T - T_0)] \tag{10}$$

where

$$Ra = \frac{\rho_0 g \alpha \Delta T D^3}{\eta_0 \kappa}$$

$$Q = \frac{Ra_i}{Ra} = \frac{\rho_0 H D^2}{\Delta T K_0}$$

and u_i is the velocity vector, $\eta(T, \tau_{yield}, I)$ is a viscosity function, T is temperature, τ_{yield} is a material yield stress, I is the second invariant of the strain rate tensor, ϵ_{ij} is the strain rate tensor, p is pressure, Ra is the Rayleigh number defined fro bottom heating, $\hat{k}$ is the vertical unit vector, ρ is the mantle density, α is the coefficient of thermal expansion, g is the gravitational acceleration, ΔT is the temperature drop across the system, D is the system depth, η_0 is a reference viscosity, κ is thermal diffusivity, Q is the

ratio of the thermal Rayleigh number defined for internal heating (Ra_i) to that defined for bottom heating, and H is internal heat generation per unit mass.

For isoviscous experiments the mantle viscosity η is independent of temperature, strain rate, and stress. For temperature- and yield stress-dependent experiments, the viscosity function has two branches [Moresi and Solomatov, 1998]. Mantle rheology remains on a temperature-dependent viscous branch for stresses below a specified value, τ_{yield}. Along this branch, the deformation mechanism is diffusion creep and the viscosity is given by:

$$\eta_{creep} = Aexp[-\theta T] \tag{11}$$

where A and θ are material parameters. For stresses above τ_{yield}, the flow law switches to a plastic branch. The yield criterion is defined by:

$$\tau_{yield} = \tau_0 + \tau_1 z \tag{12}$$

where τ_0 is the surface yield stress, τ_1 is the slope of the yield curve, and z is depth. The non-linear, effective viscosity along the plastic deformation branch is given by

$$\eta_{plastic} = \frac{\tau_{yield}}{I} \tag{13}$$

where I is the second strain-rate invariant.

Equations are solved using two versions of a community finite element code: CitCom [Moresi and Solomatov, 1995] is used for 2D Cartesian cases; CitComCU [Moresi and Gurnis, 1995] for 3D Cartesian cases. Note that this is a different code than that used by Moore [2008]. It is also different than the code used by O'Farrell and Lowman [2010].

All the numerical experiments will assume constant surface and basal temperature conditions with non-dimensional values of 0 and 1, respectively. Surface and basal velocity conditions are free slip (zero vertical velocity and free horizontal velocity). The side conditions for the 3D cases are wrap around. For 2D cases the side conditions are reflecting.

The 3D iso-viscous experiments are performed in a 4x4x1 Cartesian domain with a finite element mesh density of 256x256x64. The 2D experiments are performed in a 1x1 domain. For the iso-viscous 2D experiments, resolved solutions could be calculated using a mesh density of 64x64 (this was confirmed via convergence testing using 64x64, 96x96, and 128x128 mesh densities). This was not the case for 2D cases for temperature- and yield

stress-dependent experiments. A minimum mesh density for all cases was 128x128. For the cases run at the highest degrees of temperature-dependence and convective vigor, mesh densities of 256x256 were required (convergence testing for those cases also employed 384x384 and 512x512 density meshes).

4. Numerical Experiments: Results

Figure 2 shows the thermal field from an iso-viscous experiment. Figures 3 plots rms velocities, average surface velocities, and non-dimensional surface heat flux (Nusselt numbers Nu) from 34 such experiments with varied basal and internal heating Rayleigh numbers. Figure 4 shows horizontally averaged temperature and velocity profiles from a sub-suite of experiments. Figure 5 shows mid-depth thermal slices from the same sub-suite. All results are from times when the experiments had entered statistically steady state. This was determined by monitoring diagnostic times series outputs and convection patterns. The mid-depth slices allowed for pattern monitoring; plotted results represent time windows when the location of up-flows and down-flows may be moving relative to a mean location but the system had entered a stage where the average convective wavelength, within the model domain, was not changing.

Figure 6a compares rms velocity results to those of O'Farrell and Lowman [2010]. The consistency provides a verification test as different numerical codes were employed across the studies. The combined experiments show that a single scaling relationship cannot fit the results. This is confirmed in Figure 6b which plots numerical results against the predicted scaling trends based on Moore [2008]. The existence of different scaling regimes, across variations in a control parameter, indicates that different physical factors are influencing system behavior [Grossman and Lohse, 2000].

Increased internal heating lowers the velocity of the lower boundary layer (Figure 4), which feeds into decreased rms velocity (Figures 3 and 6a). Increased internal heating also affects the velocity of the upper boundary layer (Figure 6b). The theory of section 2 predicts that increased internal heating lowers boundary layer interaction which, in turn, lowers upper boundary layer velocity. The predictions are consistent with experimental results over the low range of internal heating (Figure 6b). The break from the theoretical trends, at higher degrees of internal heating, indicates factors not accounted for in the theory are feeding into experimental trends.

From $Q = 0$ to $Q = 3$, the system experiences mild changes in convective wavelength and planform (Figure 5). Subsequent 2D models will confirm that the initial drop in velocities, with increased internal heating, is not due to wavelength or planform changes. From $Q = 3$ to $Q = 10$, significant changes in wavelength and planform occur (Figure 5). The planform change is from linear up-flows and down-flows toward isolated and more cylindrical down-flows (similar transitions were previously documented in both numerical and laboratory convection experiments [Houseman, 1988; Weinstein and Olson, 1990]). Convective wavelength and planform affect system velocity [Schubert et al., 2001]. The theory of Moore [2008] does not explicitly account for planform changes and was fit only to 2D results. This leads to a departure from theoretical predictions (Figure 6b).

The planform change that occurs near $Q = 3$ is reflected in the slope of scaling trends and in the ratio of upper boundary layer velocity to rms velocity (Figures 3 and 6b). The ratio drops below unity at the transition to a cylindrical down-flow mode. For sheet-like down-flows, the velocity of upper boundary layer material flowing into downwellings is equal to the velocity of the down-flows. This is not the case once thermal downwellings take on a cylindrical form. To conserve radial mass flux into the down-going cylinder, the velocity in the boundary layer must decrease with distance from the center. As a result, the average velocity of the upper boundary drops.

Beyond $Q = 5$, the system experiences milder changes in wavelength and planform (Figure 5). The rms velocity continues to decrease but with a different slope (Figures 3 and 6a). At the highest degrees of internal heating, the rms velocity tends toward a flatter trend consistent with the results of Weller et al. [2016]. This change is reflected in surface heat flux trends (Figure 3). Over the lower internal heating range, surface heat flux is a weak function of internal heating. In the higher internal heating range, heat flux is an increasing function of internal heating (eq. 5). Surface heat flux increases despite the fact that the upper boundary layer velocity is decreasing and convective planforms are not changing significantly. This differs from either a basal or an internal heating end-member and from long standing expectations about the relationship between plate velocities and mantle cooling [Turcotte and Oxburgh, 1967].

Increased internal heating leads to a warmer interior mantle (Figure 4). The increased temperature across the upper boundary layer allows surface heat flux to increase despite decreasing boundary layer velocity and increasing boundary layer thickness [Moore, 2008]. The changes in wavelength and

planform, over the lower internal heating range, feed into the relatively flat heat flux trend. In the high internal heating range, when planform and wavelength shows a relative stabilization, surface heat flux increases with internal heating (eq. 5 and Figure 3).

At the highest degree of internal heating, basal heating is weak. An expectation might be that the system should then scale as an internally heated system and rms velocity should increase. This is not observed (Figure 1b, 3, and 6). At the high internal heating range, thermal profiles within the interior mantle become sub-adiabatic, with an associated change in velocity profiles (Figure 4).

A sub-adiabatic thermal profile leads to stable internal density layering (hot, low density, mantle above cold, higher density, mantle). This leads to a penetrative mode of convection that acts to lower average convective velocities. This is particularly pronounced for the lower most mantle (the velocity profiles of Figure 4 indicate that the lower mantle tends toward relative stagnation at the highest degrees of internal heating).

A strong sub-adiabatic thermal gradient also leads to an entrainment effect that acts to damp velocities. Relatively warm upper mantle is pulled down into the lower mantle by cold downwelling plumes (Figure 7). The warm material is pulled into cooler lower mantle and, as a result, there is a positive buoyancy effect that lowers the integrated negative buoyancy of the thermal down-flow.

The effect above was documented by Lowman et al. [2001] and King et al. [2002] in the context of convective re-organization events. Although it can lead to changes in convective patterns, it is operative even under situations were planforms maintain stability (Figures 5 and 7). Lowman et al. [2001] and King et al. [2002] referred to the effect as one of "trapped heat" - that is, relatively warm upper mantle developing near regions of mantle down-flow. All of our models are in statistical steady state. That is, surface heat flux and internal heat generation are in balance (i.e., there is no "trapped" heat). Despite this, the idea that increased internal mantle temperatures can lead to convective re-organization does have applicability to our results, as will be made clearer below.

The theory of Section 2 predicts that surface boundary layer velocity can decrease with increased internal heating with no changes in convective wavelength and/or planform [Moore, 2008]. To confirm this, we ran suites of 2D models that allowed constant wavelengths to be maintained over larger heating ranges than 3D models. By their nature, the 2D models also do

not allow for transitions from sheet-like to plume-like down-flow (planform changes). Figure 8 shows surface velocity results from the 2D models.

The results of Figure 8 confirm that surface velocity can decrease, with increased internal heating, independent of changes in convective wavelength or planform. They also confirm that increased internal heating leads to convective re-organization (changes in convective wavelength from a cell that fills the modeling domain to multiple cells within the domain [Schubert and Anderson, 1985]). Before a wavelength change occurs, the system experiences enhanced time-dependence. This is in line with Lowman et al. [2001] and King et al. [2002]. Time-dependence increases as a single cell configuration tends toward instability. The term "trapped heat" is less of a misnomer near those transition points as the system experiences a wavelength change that allows a statistical steady state to be re-established.

The results of Figure 8 also show that different cell wavelengths can be stable under the same parameter values (bistability). This allows convective wavelength to depend on wether the models progress through increasing or decreasing values of internal heating (hysteresis). This hysteresis/bistability is independent of temperature- and/or stress/strain rate-dependent rheology. It differs from tectonic bistability ideas, which rely on rheological effects [e.g., Crowley and O'Connell, 2012; Weller and Lenardic, 2012].

Thus far we have explored the effects of increased internal heating on thermal buoyancy effects, coupled to changes in convective wavelength/planform. Buoyancy connects to driving forces for convective motions. For convection in the Earth's mantle, and associated plate tectonic velocity, increased internal heating can also affect resisting forces. Increased internal temperature lowers internal mantle viscosity [Kohlstedt et al., 1995]. If internal viscosity provides the principal resistance to plate motions, then plate velocities can increase as mantle viscosity decreases [Tozer, 1967; 1972].

Figure 9 shows results from experiments with temperature-dependent viscosity and a yield stress formulation that allows for the dynamic formation of plate margin analogs [Moresi and Solomatov, 1998]. The bottom heated Rayleigh number can be defined using the surface viscosity (i.e., the temperature-dependent viscosity at a non-dimensional temperature of zero) or the basal viscosity (i.e., the viscosity at a non-dimensional temperature of one). The former is set to a value of 200 for all the numerical suites. The later, Ra_b, varies between the three different suites run at different degrees of temperature-dependent viscosity (i.e., different activation energies; values shown in Figure 9). The internal heating Rayleigh number based on the

viscosity at the mid-depth mantle temperature was used in Figure 9 to plot scaling trends (this temperature is not an input parameter; it was determined from model outputs once models entered a statistically steady-state). The nature of the modeling geometry insures that no planform changes are possible and all results presented maintained a domain filling, cell aspect ratio. Expected scaling trends from end-member cases of pure internal or pure bottom heating are also displayed in Figure 9 [Schubert et al., 2001].

As per iso-viscous experiments, increased internal heating leads to a hotter interior mantle with the upper mantle becoming progressively hotter than the lower mantle (Figure 9a). Unlike iso-viscous experiments, increased internal heating also leads to a decrease in average mantle viscosity and an increase in viscosity from the upper to the lower mantle. The former lowers the resistance to plate overturn [Tozer, 1967; 1972; Schubert et al., 2001]. The latter leads to a flow channelization effect in the upper mantle [Lenardic et al., 2019]. Both, on their own, tend to increase upper boundary velocity. Thus, unlike iso-viscous models, upper boundary layer velocity does not decrease with increased internal heating. None the less, the rate of velocity increase is lower than would result from purely bottom or internally heated convection (Figure 9b).

At the highest degree of internal heating, the experiments do tend toward an internal heating trend (Figure 9b). Before the asymptotic regime was reached, all of the suites transitioned to a stagnant lid mode and surface velocities dropped to zero. A transition from a plate-tectonic to a stagnant lid mode with increased internal heating has previously been attributed to decreased mantle viscosity lowering convective stress and the degree of mantle-lithosphere coupling [O'Neill et al., 2007; Stein et al., 2013; Weller et al., 2015]. Our experiments indicate that the dominant effect is related to thermal buoyancy. Increased internal heating leads to a hotter upper mantle that becomes progressively more buoyant (Figure 9a). The zone of hot upper mantle is skewed toward down-flows. This is what Lowman et al. [2001] and King et al. [2002] referred to as "trapped heat". Hot upper mantle eventually initiated a 'slab break-off' effect by lowering the negative buoyancy of mantle down-flows and by thinning the sinking upper boundary layer. Subsequent to slab break-off, the system entered into a stagnant lid mode of behavior.

5. Discussion

The results presented here demonstrate that the dynamics of mixed mode heating are not adequately captured by bottom or internally heated end-members and emphasize that boundary layer stability does not govern boundary layer thickness in the mixed (or moderate-Ra bottom-heated) case [Moore, 2008]. An implication is that surface velocity can decrease with increased levels of internal heating.

To date, the only argument presented for decreasing surface velocities, with increased internal heating, has relied on increased mantle melting generating a thicker dehydrated lithosphere which, in turn, increases plate viscosity/strength in the past [Korenaga, 2003]. Our results show that surface velocities can decrease, with increased internal heating, in an iso-viscous system, i.e., melting and rheological effects are not be the cause which leaves thermal buoyancy effects. To the best of our knowledge, this has not been demonstrated to date. A buoyancy effect is more robust as it makes no assumption as to melting and/or rheology (rheological and material melting assumptions are, by definition, phenomenological as opposed to universal; universal refers to arguments that are not dependent on phenomenological laws that apply to particular materials). Allowing for temperature-dependent mantle viscosity and weak plate boundary analogs, changes quantitative velocity scaling trends but the trends remain un-captured by theoretical ideas based on end-member cases. The deviations from end-member behavior remain connected to buoyancy effects, as opposed to being dominantly a function of rheology.

The degree to which our results relate to mantle convection and plate tectonics is a question that can not be answered in theory - it requires observational constraints. Our results would be pertinent to the Earth if, at present, mantle heating has significant contributions from both internal and basal heating and/or if there is interaction between the lower and upper thermal boundary layers of mantle convection. The former would mean that bottom or internal heating end-member scalings might not provide an adequate approximation for thermal history modeling, particularly if the mantle heating ratio has not been constant over time. The latter would mean that the assumption of a self-determined boundary layer, which has served as a corner stone for thermal history models, may lead to significant errors in modeling mantle convection generally, and in mixed-heating cases specifically.

Several studies have used hot spot swells to constrain the ratio of bottom

to internal heating in the Earth's mantle [e.g., Davies, 1988; Sleep 1990]. A recent study concludes that of the solid Earth's 43 TW of surface heat flow, 2-6 TW is associated with basal heating [Hoggard et al., 2020]. Global swell topography, mapped in that study, is consistent with lower boundary layer mantle plumes interacting with the upper boundary layer (i.e., the lithosphere). Interaction between the Earth's upper boundary layer (subducting slabs) and lower thermal boundary layer has also been argued for [e.g., Lenardic and Kaula, 1994; Labrosse, 2002; Jellinek et al., 2002]. That interaction could allow for a component of basal heating that would not manifest itself at the Earths surface via mantle plumes. It would, instead, be dissipated in heating slabs at the core-mantle boundary (for this reason, arguments against mantle plumes being the cause of mid-plate volcanism do not rule out mixed heating). The effect noted could lead to a larger component of basal heat flow than would be inferred from mid-plate swells alone. Estimates that account for this still suggest that the mantle is heated by internal and basal sources, without either dominating the other [Lay et al., 2008]. A level of mixed heating is also consistent with arguments that the thermal profile of the mantle is sub-adiabatic [Jeanloz and Morris, 1987; Bunge et al., 2001; Bunge, 2005].

It has been argued that mantle convection is driven exclusively by bottom heating [Morgan et al., 1995; 2013]. Under this view, the asthenosphere is considered a thermal inversion maintained by mantle plumes. As a result, plate cooling and mid-plate volcanism are both connected to a basal heat source. If this is the case, it argues for a large degree of lower to upper thermal boundary layer interaction. Even if the mantle is basally heated at present, this need not have been the case in the past. We now turn to paleo-constraints.

If the ratio of internal to basal heating increased in the past, then that would imply that boundary layer interaction has increased over the Earth's history and that the cooling rate of the Earth may not be adequately captured by scaling laws based on end-member cases. Models of the Earth's bulk composition can be used to constrain the percentage of radioactive elements within the mantle which can provide estimates of internal heat generation in the past [O'Neill et al., 2020]. Minimum basal heat flux constraints come from the need to maintain a geodynamo in the Earth's past [Nimmo, 2015]. Within uncertainty, the ratio of the two suggest that internal relative to basal heating has increased in the Earth's past. This is consistent with a petrological study that sought to constrain the paleo-temperatures of ambient upper mantle and

hotspot volcanic regions [Condie et al., 2016]. The study indicated that the melting temperature of volcanic rocks, consistent with formation in a mid-ocean ridge setting, increased in the Earths past while the temperature of rocks attributed to a mantle plume source remained constant. Assuming that the plume source provides a metric for temperature at or near the core mantle boundary, the two different trends are consistent with an increase in the ratio of internal to basal mantle heating in the Earth's past.

The above suggests that the results presented herein could have an influence on our understanding of the Earth's thermal and geological evolution. To date, the majority of thermal history models have used scaling relations from end-member cases and/or maintained the assumption of self-determined boundary layer dynamics. Whether or not a re-evaluation of such models, in light of our results, would lead to significant changes requires a comparative thermal history study with associated uncertainty quantification [Seales et al., 2019; Seales and Lenardic, 2020]. That type of study goes beyond the scope of this paper.

6. Conclusion

Suites of numerical convection experiments, driven by mixed heating, indicate that increased internal heating can lower convective velocities, in accord with previous studies [O'Farrell and Lowman, 2010]. Theoretical scaling analysis predicts that upper boundary layer velocity decreases, with increased internal heating, due to lowered interaction between upper and lower thermal boundary layers. Added analysis shows that changes in convective wavelength and planform augment the tendency of convective velocities to decrease with internal heating. Experiments that include temperature-dependent viscosity indicate that this, combined with weak plate boundary analogs, can change scaling trends such that velocities can increase with internal heating provided that convective wavelength and planform remain constant. The rates of increase remain lower than would be predicted based on internal of basally heated end-members and parameter windows exist over which surface velocities are independent of internal heating.

References

[1] Bunge, H. P. (2005), Low plume excess temperature and high core heat flux inferred from non-adiabatic geotherms in internally heated mantle circulation models, *Phys. Earth Planet. Inter., 153*, 3-10.

[2] Bunge, H. P., Y. Ricard, and J. Matas (2001), Non-adiabaticity in mantle convection, *Geophys. Res. Lett., 28*, 879-882.

[3] Castaing, B. G. Gunaratne, F. Heslot, L. Kadanoff, A. Libchaber, S. Thomae, X. Z. Wu, A. Zaleski, and G. Zanetti (1989), Scaling of hard thermal turbulence in Rayleigh-Benard convection, *J. Fluid Mech., 204*, 1-30.

[4] Choblet, G. (2012), On the scaling of heat transfer for mixed heating convection in a spherical shell, *Phys. Earth Planet. Inter., 206-207*, 31-42.

[5] Choblet, G., and E. M. Parmentier (2009), Thermal convection heated both volumetrically and from below: Implications for predictions of planetary evolution, *Phys. Earth Planet. Inter., 173*, 290-296.

[6] Condie, K. C., Aster, R. C., and Van Hunen, J. (2016), A great thermal divergence in the mantle beginning 2.5 Ga: Geochemical constraints from greenstone basalts and komatiites, *Geoscience Frontiers, 7(4)*, 543-553, doi:10.1016/j.gsf .2016.01.006.

[7] Conrad, C.P. and Hager, B.H., (1999), The thermal evolution of an Earth with strong subduction zones, *Geophys. Res. Lett., 26(19)*, 3041-3044.

[8] Crowley, J.W., and O'Connell, R.J., (2012), An analytic model of convection in a system with layered viscosity and plates, *Geophys. J. Int. 188*, 61-78. https://doi.org/10.1111/j. 1365-246X.2011.05254.x.

[9] Davies, G. F. (1980), Thermal histories of convective Earth models and constraints on radiogenic heat production in the Earth, *J. Geophys. Res., 85(B5)*, 2517-2530, doi:10.1029/JB085iB05p02517.

[10] Davies, G. F. (1988), Ocean bathymetry and mantle convection. 1. Large- scale flow and hotspots, *J. Geophys. Res., 93 (B9)*, 10,467-10,480.

[11] Deschamps, F., P. J. Tackley, and T. Nakagawa (2010), Temperature and heat flux scalings for isoviscous thermal convection in spherical geometry, *Geophys. J. Int., 182*, 137-154.

[12] Deschamps, F., C. Yao, P. J. Tackley, and C. Sanchez-Valle (2012), High Rayleigh number thermal convection in volumetrically heated spherical shells, *J. Geophys. Res., 117*, E09006, doi:10.1029/2012JE004090.

[13] Grasset, O., and Parmentier, E. M. (1998), Thermal convection in a volumetrically heated, infinite Prandtl number fluid with strongly temperature-dependent viscosity: implications for planetary thermal evolution, *J. Geophys. Res. 103*, 171-181.

[14] Grossman, S. and Lohse, D. (2000), Scaling in thermal convection: a unifying view, *J. Fluid. Mech. 407*, 27-56.

[15] Hoggard, M.J., R. Parnell-Turner, and N. White (2020), Hotspots and mantle plumes revisited: Towards reconciling the mantle heat transfer discrepancy, *Earth Planet. Sci. Lett., 542*, 116317, https://doi.org/10.1016/j.epsl.2020.116317.

[16] Howard, L. N. (1966), Convection at high Rayleigh number, in *Proc. 11th Cong. Appl. Mech.*, edited by H. Gortler, pp. 1109 - 1115, Springer-Verlag, Berlin, Germany.

[17] Houseman, G. (1988), The dependence of convection planform on mode of heating, *Nature, 332*, 346-349, 1988.

[18] Jaupart, C., S. Labrosse, and J. C. Mareschal (2007), Temperatures, heat and energy in the mantle of the Earth, *Treatise on Geophysics, 7*, 253-303.

[19] Jeanloz, R., and S. Morris (1987), Is the mantle geotherm subadiabatic?, *Geophys. Res. Lett., 14*, 335-338.

[20] Jellinek, A.M., A. Lenardic, M. Manga (2002), The influence of interior mantle temperature on the structure of plumes: heads for Venus, tails for Earth, *Geophys. Res. Lett. 29*, doi:10.1029/2001GL014624.

[21] Kadanoff, L. P. (2001), Turbulent heat flow: structures and scaling, *Phys. Today 54*, 34-39.

[22] King, S.D., J.P. Lowman, J.P., and C.W. Gable (2002), Episodic tectonic plate reorganizations driven by mantle convection, *Earth Planet. Sci. Lett., 203*, 83-91.

[23] D.L. Kohlstedt, B. Evans, S.J. Mackwell (1995), Strength of the lithosphere: constraints imposed by laboratory experiments, *J. Geophys. Res. 100*, 17587-17602.

[24] Korenaga, J. (2003), Energetics of mantle convection and the fate of fossil heat, *Geophys. Res. Lett., 30*, 1437, doi:10.1029/2003GL016982.

[25] Korenaga, J. (2017), Pitfalls in modeling mantle convection with internal heat production, *J. Geophys. Res., 122*, 4064-4085, doi:10.1002/2016JB013850.

[26] Labrosse, S. (2002), Hotspots, mantle plumes and core heat loss, *Earth Planet. Sci. Lett., 199*, 147-156.

[27] Lenardic, A., and W.M. Kaula (1994), Tectonic plates, D" thermal structure, and the nature of mantle plumes, *J. Geophys. Res.-B, 99,* 15,697-15,708.

[28] Lenardic, A., and L. Moresi (2003), Thermal convection below a conducting lid of variable extent: Heat flow scalings and two-dimensional, infinite Prandtl number numerical simulations, *Phys. Fluids, 15(2)*, 455 - 466.

[29] Lenardic, A., M. Weller, T. Hoink, and J. Seales (2019), Toward a Boot Strap Hypothesis of Plate Tectonics: Feedbacks Between Tectonics, Mantle Viscosity, and The Wavelength of Mantle Convection, *Phys. Earth Planet. Int.,296,* https://doi.org/10.1016/j.pepi.2019.106299, 2019.

[30] Lay, T., J. Hernlund, and B. Buffett (2008), Core-mantle boundary heat flow, *Nature Geoscience, 1 (1)*, 25-32.

[31] Lowman, J.P., S.D. King, and C.W. Gable (2001), The influence of tectonic plates on mantle convection patterns, temperature and heat flow, *Geophys. J. Int., 146*, 619-636.

[32] Moore, W. B. (2008), Heat transport in a convecting layer heated from within and below, *J. Geophys. Res., 113*, B11407, doi:10.1029/2006JB004778.

[33] Moresi, L., and Gurnis, M. (1995), Constraints on the lateral strength of slabs from three-dimensional dynamic flow models, *Earth Planet. Sci. Lett., 138*, 15-28. https://doi.org/ 10.1016/0012-821X(95)00221-W.

[34] Moresi, L., and V. S. Solomatov (1995), Numerical investigations of 2D convection with extremely large viscosity variations, *Phys. Fluids, 7*, 2154-2162.

[35] Morgan, J.P., Morgan, W.J., Zhang, Y.-S. , Smith, W.H.F. (1995), Observational hints for a plume-fed, suboceanic asthenosphere and its role in mantle convection, *J. Geophys. Res. 100*, 12753-12768.

[36] Morgan, J.P., Hasenclever, J., Shi, C. (2013), New observational and experimental evi- dence for a plume-fed asthenosphere boundary layer in mantle convection, *Earth Planet. Sci. Lett., 366*, 99-111.

[37] Moresi, L., and Solomatov, V.S. (1998), Mantle convection with a brittle lithosphere: thoughts on the global tectonic styles of the Earth and Venus, *Geophys. J. Int., 133(3)*, 669-682, doi:10.1046/j.1365-246X.1998.00521.x.

[38] Nimmo, F. (2015), Energetics of the core, In: *Treatise on Geophysics* (edited by G. Schubert), vol. 8, chap. 2. Elsevier, Amsterdam, 2 edn.

[39] O'Farrell, K. A., and J. P. Lowman (2010), Emulating the thermal structure of spherical shell convection in plane-layer geometry mantle convection models, *Phys. Earth Planet. Int., 182*, 73-84, doi:10.1016/j.pepi.2010.06.010.

[40] O'Farrell, K. A., J. P. Lowman, and H.-P. Bunge (2013), Comparison of spherical shell and plane-layer mantle convection thermal structure in viscously stratified models with mixed-mode heating: Implications for the incorporation of temperature-dependent parameters, *Geophys. J. Int., 192*, 456-472, doi:10.1093/gji/ggs053.

[41] O'Neill, C., Lenardic, A., Moresi, L., Torsvik, T., Lee, C.A. (2007), Episodic Precambrian subduction, *Earth Planet. Sci. Lett. 262*, 552-562. (doi:10.1016/j.epsl.2007.04.056)

[42] O'Neill, C., O'Neill, H.S.C. and Jellinek, A.M. (2020), On the Distribution and Variation of Radioactive Heat Producing Elements

Within Meteorites, the Earth, and Planets, *Space Sci Rev 216*, 37, https://doi.org/10.1007/s11214-020-00656-z.

[43] Schubert, G., D. Stevenson, and P. Cassen (1980), Whole Planet Cooling and the Radiogenic Heat Source Contents of the Earth and Moon, *J. Geophys. Res., 85(B5)*, 2531-2538.

[44] Schubert, G. and C. Anderson (1985), Finite element calculations of very high Rayleigh number thermal convection, *Geophys. J. Roy. Astron. Soc., 80*, 575-601.

[45] Schubert, G, D. L. Turcotte, and P Olsen (2001), *Mantle Convection in the Earth and Planets*, 956 pp., Cambridge Univ. Press, Cambridge.

[46] Seales, J., A. Lenardic, and W.B. Moore (2019), Assessing the Intrinsic Uncertainty and Structural Stability of Planetary Models: 1) Parameterized Thermal-Tectonic History Models, *J. Geophys. Res.,124,* https://doi.org/10.1029/2019JE005918.

[47] Seales, J., and A. Lenardic (2020), Uncertainty Quantification for Planetary Thermal History Models: Implications for Hypotheses Discrimination and Habitability Modeling, *Astrophys. J., 893:114,* https://doi.org/10.3847/1538-4357/ab822b.

[48] Shahnas, M. H., J. P. Lowman, G. T. Jarvis, and H.-P. Bunge (2008), Convection in a spherical shell heated by an isothermal core and internal sources: Implications for the thermal state of planetary mantles, *Phys. Earth planet. Int., 168*, 6-15.

[49] Sinha, G., and S. L. Butler (2007), On the origin and significance of subadiabatic temperature gradients in the mantle, *J. Geophys. Res., 112*, B10406, doi:10.1029/2006JB004850.

[50] Sleep, N. H. (1990), Hotspots and mantle plumes: Some phenomenology, *Geology, 95 (B5)*, 6715-6736.

[51] Sotin, C., and S. Labrosse (1999), Three-dimensional thermal convection in an iso-viscous, infinite Prandtl number fluid heated from within and from below: Applications to the transfer of heat through planetary mantles, *Phys. Earth Planet. Inter., 112(3-4)*, 171-190.

[52] Stein, C., J.P. Lowman, and U. Hansen, (2013), The influence of mantle internal heating on lithospheric mobility: Implications for super-Earths, *Earth Planet. Sci. Lett., 361*, 448-459, 10.1016/j.epsl.2012.11.011.

[53] Tozer, D. C. (1967), Towards a theory of thermal convection in the mantle, in *The Earth's Mantle*, edited by T. F. Gaskell, pp. 325-353, Academic Press, London, U.K.

[54] Tozer, D.C. (1972), The present thermal state of the terrestrial planets, *Phys. Earth Planet. Inter., 6*, 182-197.

[55] Turcotte, D. L., and E. R. Oxburgh (1967), Finite amplitude convection cells and continental drift, *J. Fluid Mech., 28*, 29-42.

[56] Turcotte, D. L., and G. Schubert (1982), *Geodynamics: Applications of Continuum Physics to Geological Problems*, 450 pp., John Wiley, Hoboken, N. J.

[57] Weinsten, S.A., P.L. Olson, and D.A. Yuen (1989), Time-dependent large aspect-ratio convection in the Earth's mantle, *Geophys. Astrophys. Fluid. Dyn., 47,* 157-197.

[58] Weinsten, S.A., and P.L. Olson (1990), Planforms in thermal convection with internal heat sources at large Rayleigh and Prandtl numbers, *Geophys. Res. Lett., 17,* 239-242.

[59] Weller, M., and A. Lenardic (2016a), The Energetics and Convective Vigor of Mixed-mode Heating: Velocity Scalings and Implications for the Tectonics of Exoplanets, *Geophys. Res. Lett., 43,* doi:10.1002/2016GL069927.

[60] Weller, M., Lenardic, A. (2012), Hysteresis in mantle convection: plate tectonics systems, *Geophys. Res. Lett. 39*, L10202. (doi:10.1029/2012GL051232).

[61] Weller, M., Lenardic, A., O'Neill, C. (2015), The effects of internal heating and large scale climate variations on tectonic bistability in terrestrial planets, *Earth Planet. Sci. Lett. 420*, 85-94. (doi:10.1016/j.epsl.2015.03.021).

[62] Weller, M., A. Lenardic, and W.B. Moore (2016b), Scaling Relationships for Mixed Heating Convection in Planetary Interiors: Isoviscous Spherical Shells, *J. Geophys. Res.-Solid Earth, 121,* doi:10.1002/2016JB013247, 2016.

[63] Wolstencroft, M., J. H. Davies, and D. R. Davies (2009), Nusselt-Rayleigh number scalingfor a spherical shell Earth mantle simulation up to a Rayleigh number of 10e9, *Phys. Earth Planet. Int., 176*, 132-141.

Acknowledgements

All the data for this paper is provided within the publication pages. The data was generated via numerical calculations performed using open source, community codes available through https://geodynamics.org/cig/. The input files from our numerical experiments, which can be used to reproduce our results, can be found at https://github.com/jds16/MixedHeatingVelocities.

Figure 1 Results from the numerical experiments of (a) O'Farrell and Lowman [2010] and (b) Weller et al. [2016].

Figure 2 Thermal field from an isoviscous experiment in a 4x4x1 domain.

Figure 3 Upper boundary layer velocities, rms velocities, and surface heat flux outputs from suites of mixed heating isoviscous experiment in a 4x4x1 domain.

Figure 4 Horizontally averaged vertical temperature and velocity profiles from a sub-suite of experiments from Figure 3.

Figure 5 Mid-depth thermal field images from a sub-suite of experiments from Figure 3.

Figure 6 (a) A comparison of rms velocities from O'Farrell and Lowman [2010] and from our own mixed heating isoviscous experiments in a 4x4x1 domain. (b) A comparison of surface velocity predictions from the theory of Moore [2008] to results from numerical experiments.

Figure 7 Mid-depth thermal field (top), a vertical thermal slice with velocity arrows (middle), and plots of lateral temperatures and vertical velocities (bottom) from a mixed heating isoviscous experiment in a 4x4x1 domain..

Figure 8 Results from isoviscous, 2D experiments. Circles and squares show mean values from statistically steady-state experiments. Lines show variations about mean values (again, from time windows over which the experiments are in a statistically steady-state. The majority of experiments used the steady-state thermal fields from a lower heating ratio case as an initial condition. The exceptions are the cases labelled under "bistabilty" which used the steady-state thermal fields from a higher heating ratio case as an initial condition.

Figure 9 Results from 2D experiments with temperature- and yield stress-dependent viscosity. The surface value of the lithosphere yield stress, τ_0, is 3.0; The slope of the yield curve, τ_0, is 6.0; The bottom heated Rayleigh number, based on surface viscosity, is 200. (a) Thermal fields from select experiments. (b) Surface velocities from a suite of experiments with variable degrees of internal heating and activation energies. The dashed blue line is the trend based on classic scaling ideas for purely internally heated convection. The dashed red line is the trend based on classic scaling ideas for purely bottom heated convection.

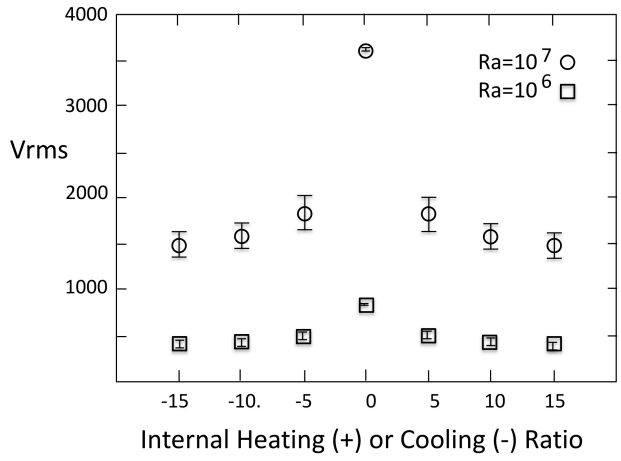

Figure 1a

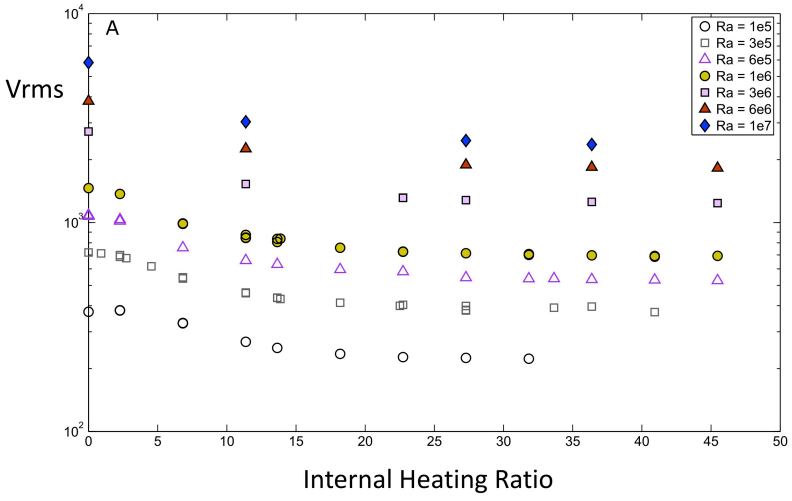

Figure 1b

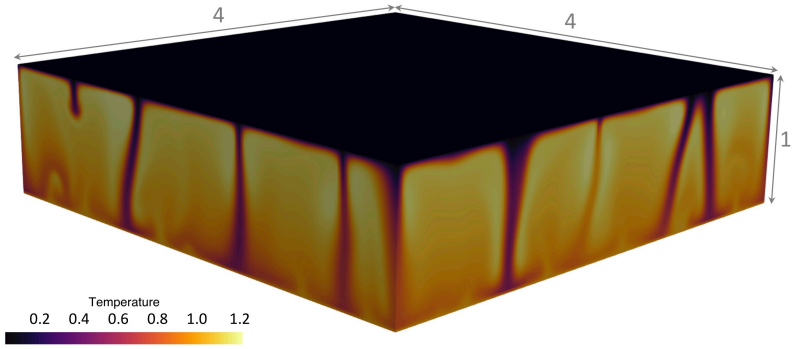

Figure 2

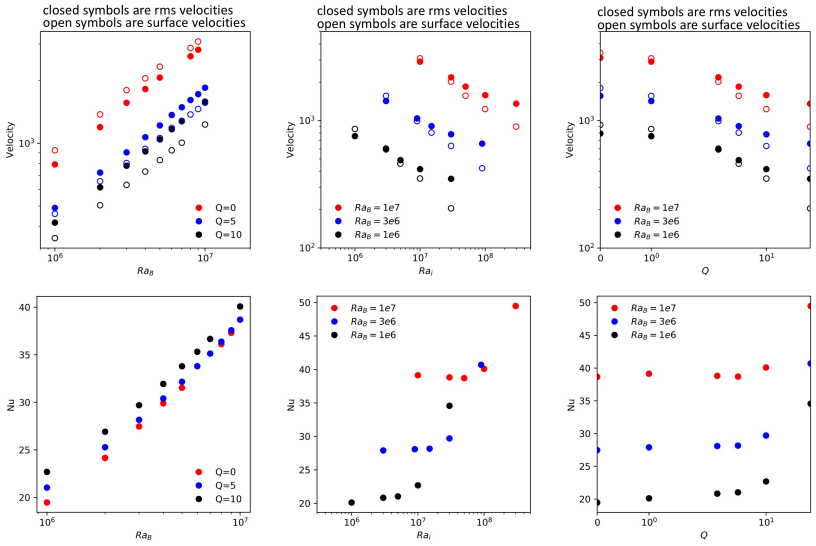

Figure 3

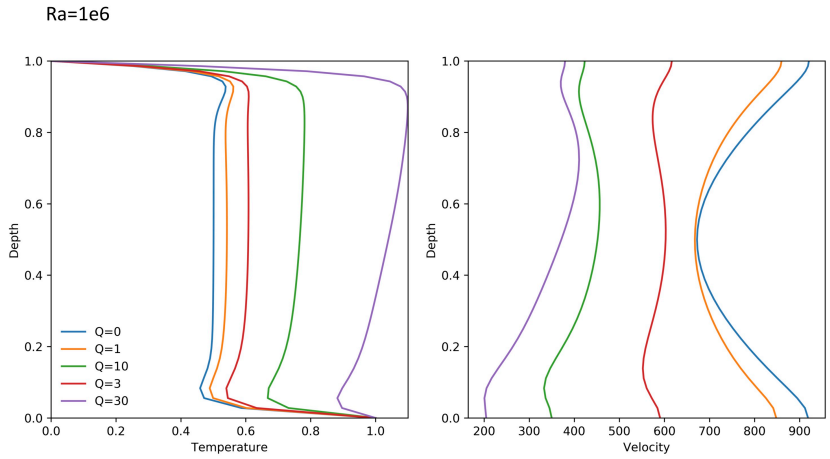

Figure 4

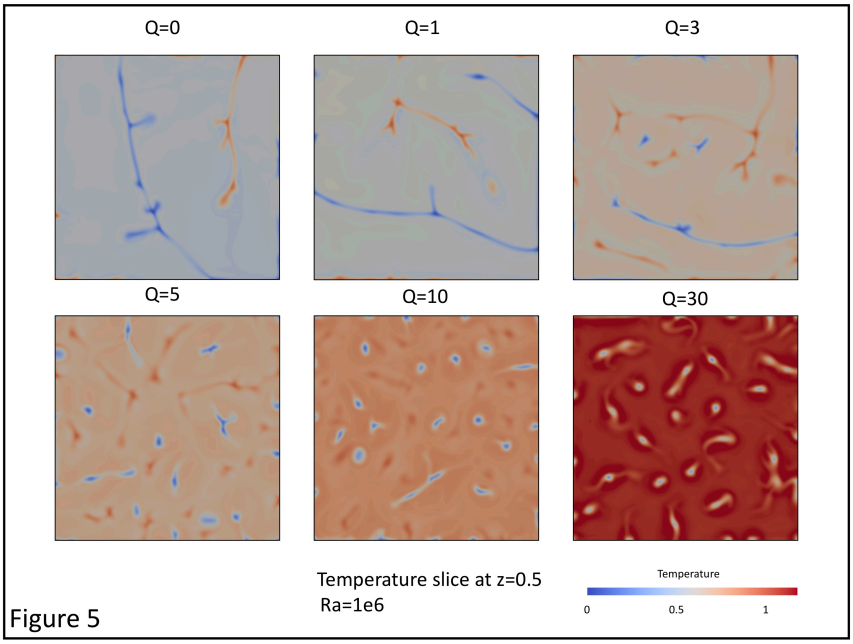

Figure 5

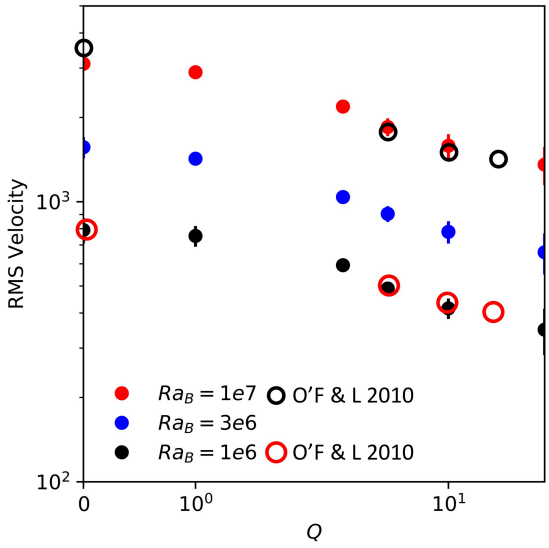

Figure 6a

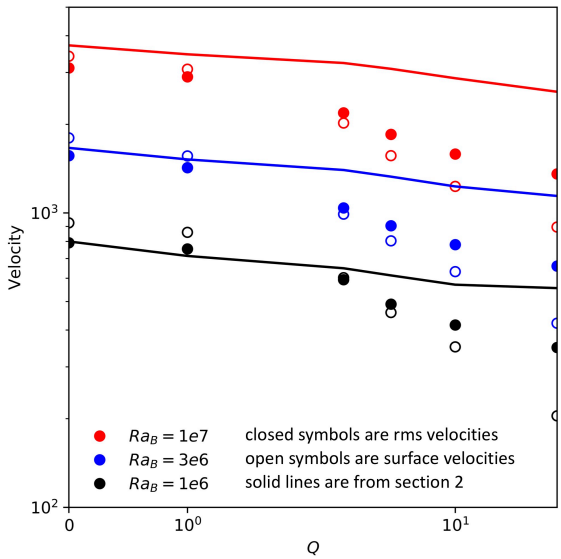

Figure 6b

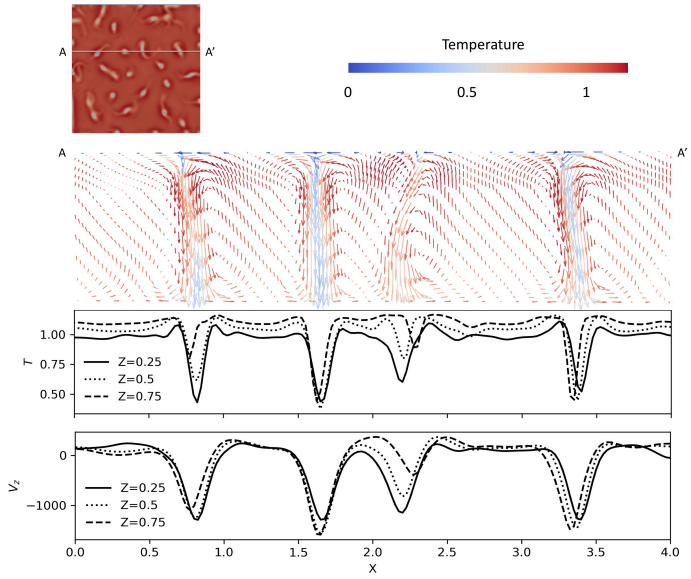

Figure 7

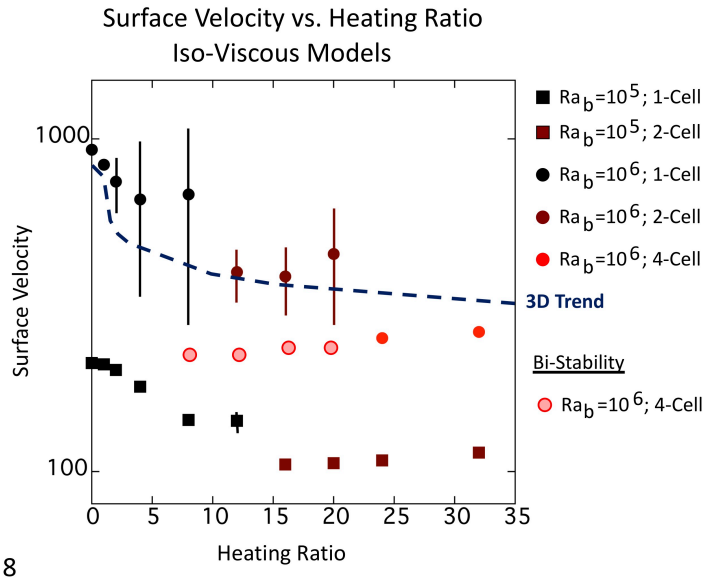

Figure 8

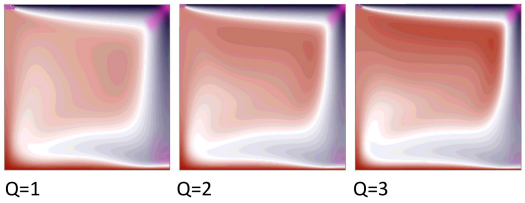

Figure 9a

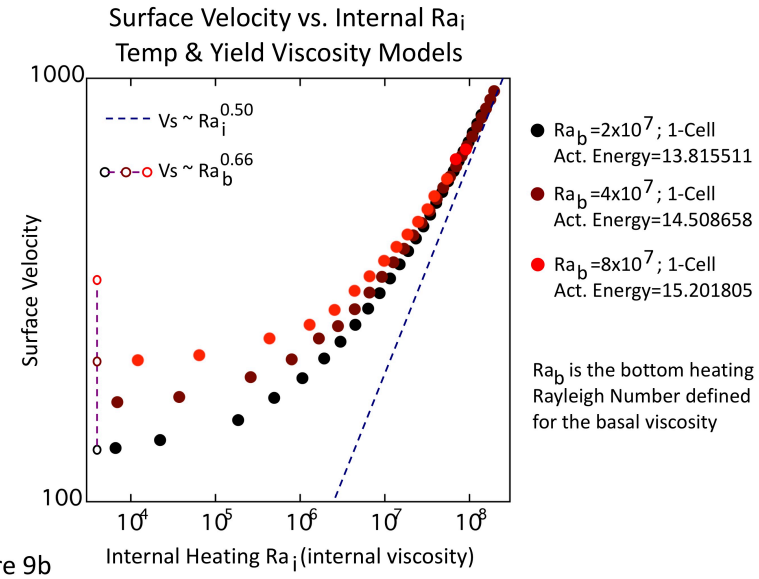

Figure 9b